Enhancing 3-D Land Seismic Data Using Nonlinear Beamforming Based on the Efficiency-Improved Genetic Algorithm

Yimin Sun, Ilya Silvestrov, and Andrey Bakulin

***Abstract*—Seismic data acquired in a desert environment often have a low signal-to-noise ratio, posing a significant challenge to seismic processing, imaging, and inversion. Nonlinear beamforming is one effective method that uses local second-order mathematical operators to describe seismic events and then enhance them. However, estimating the operator coefficients from input data is a nonlinear and compute-intensive optimization problem. We propose a new method for this estimation based on a recently developed efficiency-improved genetic algorithm. We demonstrate that it delivers an excellent balance between improved data quality and computational efficiency. We also introduce a "spatial consistency" feature to further speed up the algorithm by using available nonlinear-beamforming operators as initial trial solutions for the neighboring data ensembles. These findings are supported by applying the new approach to land seismic datasets from the desert environment.**

***Index Terms*—Approximation algorithm, geophysical signal processing, genetic algorithm (GA), seismic wave, signal restoration.**

I. Introduction

SEISMIC exploration uses seismic waves to retrieve geological information about the subsurface. On land, the waves are emitted by special vibrational or explosive sources and are recorded by receivers sensitive to displacements of ground. Fig. 1 shows an example of a seismic exploration study and a slice of a depth velocity model that needs to be reconstructed from seismic waves. In practice, three-dimensional (3-D) seismic acquisitions are used, where spatial grids of sources and receivers are laid on the ground. Fig. 2(a) shows a simple portion of such a grid, in which sources and receivers are placed as two orthogonal lines and form a cross-spread seismic gather. In the past, several nearby sources or receivers were summed or grouped to strengen the recorded signals and to improve the quality of seismic data directly in a field. Nowadays, denser grids of sources and receivers are used without such grouping to better preserve detailed information about the subsurface [1]. Modern acquisition leads to data with weaker signals, which require additional processing and enhancement. As the conventional seismic data processing toolbox is not designed for such data, today's seismic industry faces challenges in dealing with massive but low signal-to-noise ratio (SNR) data. Hence, a new suite of algorithms and methods dedicated to modern 3-D land seismic data is required.

Nonlinear beamforming (NLBF) is a recently proposed technology [2] that enhances 3-D land seismic data quality. It uses a local traveltime operator, which is a second-order mathematical operator with five unknown coefficients, to describe a seismic wavefront locally. NLBF consists of two main steps [3]. The first step, which is the topic of this work, estimates these five unknown coefficients of local traveltime operators from input data. The second step accomplishes stacking nearby traces guided by the estimated local traveltime operators to improve the data's SNR. Such an approach is similar to some other algorithms used in seismic data processing (common-reflection-surface (CRS) [4] and multifocusing [7]), where analogous sets of coefficients need to be estimated.

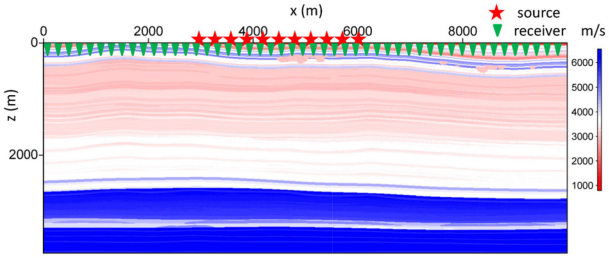

Fig. 1. Seismic exploration experiment with the sources marked as the red stars and the receivers marked as the green triangles located on the ground. The shown subsurface velocity model, which is extracted from the SEAM Arid model [29], is used to generate data for the synthetic example presented in this study.

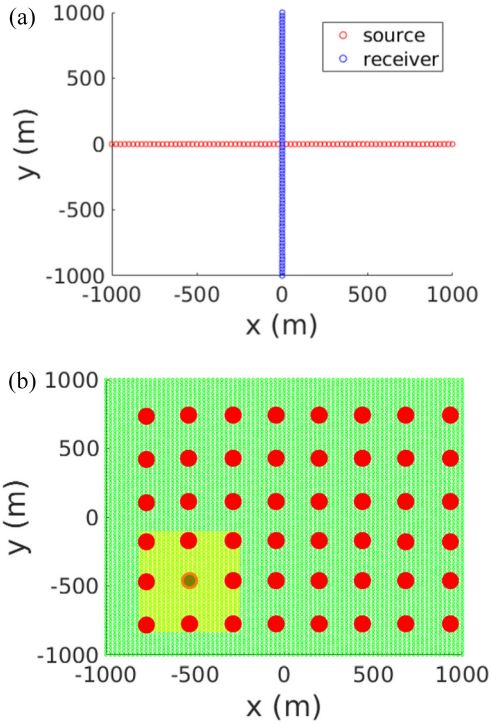

Fig. 2. (a) One source line and one receiver line of a 3-D orthogonal seismic acquisition form a cross-spread domain. (b) Actual seismic traces for shot and receiver pairs in the cross-spread domain are marked by the green dots, and the red dots mark the NLBF parameter traces. The yellow area illustrates the spatial aperture of a particular NLBF parameter trace, which is denoted by the red-circled blue dot.

Manuscript received 21 June 2021; revised 30 November 2021; accepted 28 January 2022. Date of publication 7 February 2022; date of current version 3 October 2022. *(Corresponding author: Yimin Sun.)*

Yimin Sun is with the Aramco Research Center–Delft, Aramco Overseas Company, 2628 ZD Delft, The Netherlands (e-mail: sun.delft@gmail.com).

Ilya Silvestrov and Andrey Bakulin are with the EXPEC Advanced Research Center, Saudi Aramco, Dhahran 31311, Saudi Arabia.

Digital Object Identifier 10.1109/TEVC.2022.3149579

Although parameter estimations are highly nonlinear problems, considering the computation burdens, previous NLBF implementations have used the so-called 2+2+1 approach, a local search solver breaking the 5-D optimization problem into three problems with smaller dimensions [2], [3]. In addition, 2-D searches in 2+2+1 utilize only a subset of the ensemble data. This approximation solution often delivers suboptimal results, so we expect improved results from an efficient global optimization solver. The efficiency-improved genetic algorithm (eGA) is a recently proposed global optimization method [5], [6], and its efficacy has been systematically demonstrated on both multimodal functions and a 2-D CRS problem [6]. We also employ a particular feature of local traveltime operators in NLBF, named "spatial consistency," to further improve solution efficiency. We refer to our new method as NLBF+eGA throughout the remainder of this article.

The remainder of this article is organized as follows. Section II describes the NLBF+eGA method in detail. Section III introduces three control methods that will be used later for performance comparisons with the NLBF+eGA method. Section IV applies the NLBF+eGA method to two datasets for data-quality enhancement. Section V discusses the benefit of introducing the "spatial consistency" feature into the NLBF+eGA method via comparison studies. Finally, Section VI concludes this article.

II. NLBF+eGA Method

The NLBF method assumes that the kinematic wavefront of a seismic event can be locally approximated by a local second-order traveltime operator [2]

$$\begin{aligned}\Delta t(x, y; x_0, y_0) &= t(x, y) - t(x_0, y_0) \\ &= A \cdot (x - x_0) + B \cdot (y - y_0) + C \cdot (x - x_0) \cdot (y - y_0) \\ &\quad + D \cdot (x - x_0)^2 + E \cdot (y - y_0)^2 \end{aligned} \tag{1}$$

where $t(x, y)$ is the travel time of the trace located at (x, y) in a seismic gather; $t(x_0, y_0)$ is the travel time of the NLBF parameter trace located at (x_0, y_0); and the coefficients $\{A, B, C, D, E\}$ are the unknown operator parameters for a seismic event centered at $t(x_0, y_0)$. Rigorously speaking, these coefficients should be mathematically written as $\{A(x_0, y_0, t), B(x_0, y_0, t), C(x_0, y_0, t), D(x_0, y_0, t), E(x_0, y_0, t)\}$ since they are functions of both spatial location and time. For convenience, we present these parameters by $\{A, B, C, D, E\}$ for the rest of this study.

The NLBF method retrieves a set of coefficients $\{A, B, C, D, E\}$ at $t(x_0, y_0)$ by maximizing a semblance-type cost function

$$S(x_0, y_0) = \frac{\sum_{j=1}^{N} \left\{ \sum_{i=1}^{M} u\left[x_i, y_i; t_j(x_0, y_0) + \Delta t(x_i, y_i; x_0, y_0)\right] \right\}^2}{M \sum_{j=1}^{N} \sum_{i=1}^{M} \left\{ u\left[x_i, y_i; t_j(x_0, y_0) + \Delta t(x_i, y_i; x_0, y_0)\right] \right\}^2} \tag{2}$$

where $u(x_i, y_i; t)$ represents a time sample of the trace located at (x_i, y_i) in seismic data, M is the total amount of traces inside the spatial aperture of the local traveltime operator, and N is the total amount of time samples inside the temporal aperture of the local traveltime operator [3]. Note that (2) is highly multimodal, so its smoothness is not guaranteed, making gradient-based optimization approaches nonapplicable. A commonly used 3-D prestack data domain for the NLBF method is the cross-spread domain, as shown in Fig. 2(a). NLBF parameter traces are defined as regularly distributed traces located in a 3-D prestack data domain. Fig. 2(b) further illustrates how NLBF parameter traces are organized in the 3-D cross-spread domain. The red dots are the locations of NLBF parameter traces. The yellow area illustrates the spatial aperture of a particular NLBF parameter trace marked by the red-circled blue dot.

Detailed discussions on determining search ranges for the coefficients $\{A, B, C, D, E\}$ are beyond the scope of this article, and readers interested in this topic can refer to [3]. In short, they are geology related, and for NLBF problems, they are *apriori* information entered by end users.

It is a highly nonlinear problem to retrieve the set of unknown coefficients $\{A, B, C, D, E\}$ at $t(x_0, y_0)$ through maximizing the semblance defined in (2). Genetic algorithms (GAs) [8] are a popular tool for solving general nonlinear problems. They have been researched from a wide variety of perspectives, including the coding scheme [9], the crossover scheme [10]–[12], the mutation scheme [11], [14], the evolution scheme [13], the balance between exploitation and exploration [15], [16], the solution diversity [17]–[19], etc. GAs have also found wide applications in the field of geophysics, such as building migration velocity models [20], extracting structure-based geoelectric models [21], estimating common-focus-point operators for near-surface layer replacement [22]–[24], carrying out 1-D elastic full-waveform inversion [25], optimizing statics for a complex near surface [26]–[28], etc. Despite the success of GAs in general, in reality, its convergence speed remains a challenge. We recently proposed an eGA [5], [6]. Its efficacy and robustness have been systematically demonstrated using both analytical multimodal test functions and a 2-D CRS problem. In a nutshell, eGA uses a modified island model to secure a robust global search capability, a self-adaptive differential evolution (SADE) fine-tuning scheme to achieve a good local search capability, and a local exhaustive search method to overcome the premature-convergence challenge. As mentioned before, the NLBF method is somewhat similar to the CRS method, so our previous successful application of eGA on a 2-D CRS problem gives us confidence in using it to efficiently estimate local traveltime operators in NLBF via maximizing the semblance defined in (2).

Most seismic events of interest lie in the so-called far field, meaning that a wave-propagation distance between a source and a receiver is much larger than one wavelength of the source wavelet. As a consequence, wavefronts should smoothly and gradually vary between neighboring locations. Since local traveltime operators describe wavefront kinematics, operators at nearby NLBF parameter traces should also change gradually. This particular feature of neighboring local traveltime operators can further improve the computation efficiency of the NLBF+eGA method, and we refer to it as "spatial consistency." In the NLBF+eGA method, once we finish estimating one set of parameters for a specific NLBF parameter trace, we use them as the initial values for the neighboring NLBF parameter trace. As far as we know, NLBF+eGA is the first algorithm that exploits the feature of spatial consistency in far-field seismic data to speed up the computation efficiency for wavefront-kinematic operators.

The choice of eGA control parameters has already been explained in detail in [6]. One advantage of eGA is that its performance is quite robust without tedious control-parameter tuning. In the NLBF+eGA method, we set the control parameters of eGA as follows: the amount of islands is 2; the frequency to carry out communications between islands is every three generations; the maximum and the minimum population size are 10 and 5, respectively; the local exhaustive search method is applied for every five generations and the threshold improvement ratio R_p is 0.01. In each island, the maximum and the minimum crossover probability are 0.7 and 0.3, and the maximum and the minimum α ratio in the BLX-α crossover operator are 0.8 and 0.2. The maximum and the minimum mutation probability are 0.1 and 0.01, and the maximum and the minimum mutation ratio β are 0.9 and 0.1. SADE is applied for every seven generations.

Each time, ten random pairs of members are used with the initial scaling factor set at 10.0 and the maximum iteration number set at 3. The maximum number for evolution generations in eGA is set at either 30 or 60, depending upon input data quality. The convergence condition for the NLBF+eGA method is either of the following two.

1) The number of evolution generations has reached the maximum number of evolution generations.
2) The fitness, defined by (2), of the current best member in all islands is smaller than $(1 + R_p)$ times of the fitness of the best member in all islands ten generations ago.

III. Control Methods

In order to demonstrate the efficacy and efficiency of our NLBF+eGA method, we introduce several control methods in this section, which will be used for performance comparisons with the NLBF+eGA method in the next section.

The first control method is the 2+2+1 local search method [2], [3] mentioned in the INTRODUCTION section. For each point (x_0, y_0), this method first finds the optimal values of $\{A, D\}$ by a brute-force search using a subset of data extracted along the y-direction. Likewise, during the next step, it searches for the optimal values of $\{B, E\}$ using another subset extracted along the x-direction. Finally, it finds the optimal value of C using a complete set of data after fixing previously estimated values of $\{A, B, D, E\}$. Although such a scheme is sometimes acceptable for practical applications, it is prone to converge to a local minimum instead of a global one, especially on the data with a low signal-to-noise ratio.

The second control method is the 5-D brute-force search method. As the name suggests, we discretize the search ranges of parameters A–E by small steps, evaluate all possible parameter combinations, and finally, pick out the best result as the final solution. Although this method can guarantee the result to be the ground truth if the discretization steps are small enough, computation time is a huge challenge in reality.

The third control method is the adaptive simulated annealing (ASA) method [30], an advanced variant of the simulated annealing method. ASA has found a wide range of practical applications, and it contains more than 100 control parameters. The following control parameters are tuned in this work, while the rest are left with default values: the maximum number of states accepted before quitting is 1000; the maximum number of states generated before quitting is 3000; the maximum number of repetitive invalid generated states is 1000; the smallest ratio of accepted to generated states is 0.0001; no tangents are calculated for reannealing; the penalty weight is 1000; and the maximum number of iterations for the cost function is 500.

IV. Examples

In this section, we use two examples to demonstrate the practical value of the NLBF+eGA method. All computations are carried out on the same platform equipped with 2 CPUs (14 threads/CPU, 2.40 GHz) and 256-GB memory. All codes are written in C++ and parallelized via OpenMP directives to exploit all available CPU cores.

The first is a 2-D synthetic example. The velocity model used to generate the corresponding synthetic data is shown in Fig. 1. This 2-D model is a slice extracted from the SEAM Arid velocity model [29]. The density slice is also taken from the same Arid model (not shown). We use the acoustic equation and apply finite-difference modeling for data simulation, and relevant simulation parameters are as follows: the grid spacing is 0.625 m × 0.625 m; both sources and receivers are located near the surface at $z = 0.625$ m; we use an absorption boundary condition at the surface, so our data contain no free-surface related multiples. The sources are placed between 3000 and 6000 m along the x-direction, and the receivers are distributed between 0 and 10 000 m. Both source and receiver intervals are 25 m.

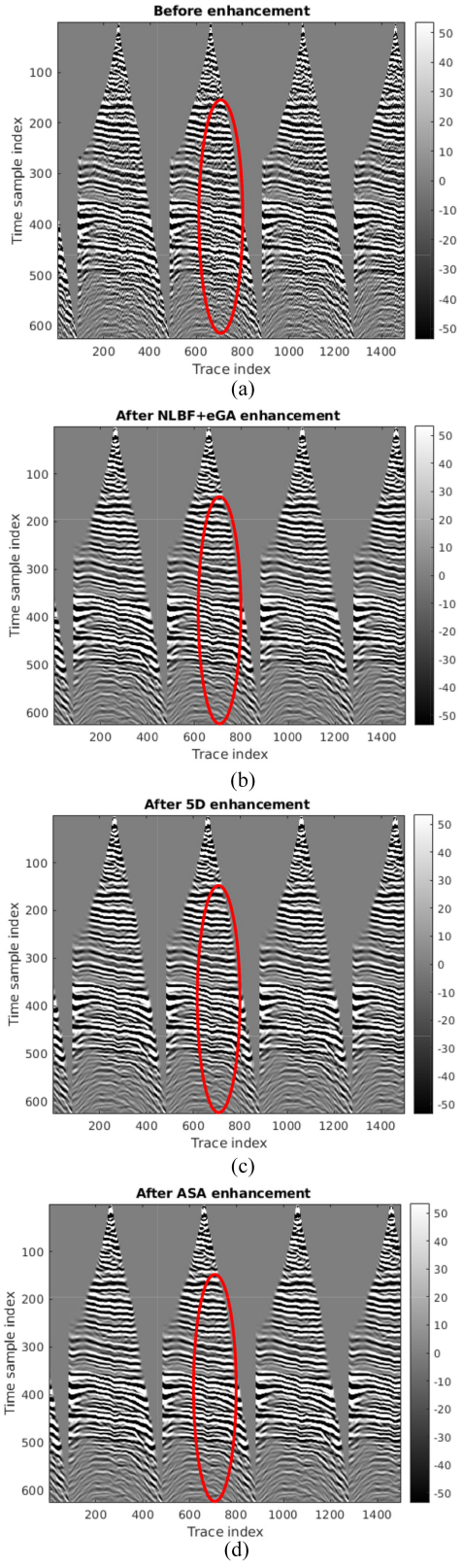

Fig. 3. (a) Several NMO-corrected raw gathers from neighboring receiver lines. The same gathers after enhancement by (b) NLBF+eGA method, (c) conventional NLBF with the 5-D brute-force search method, and (d) conventional NLBF with the ASA method.

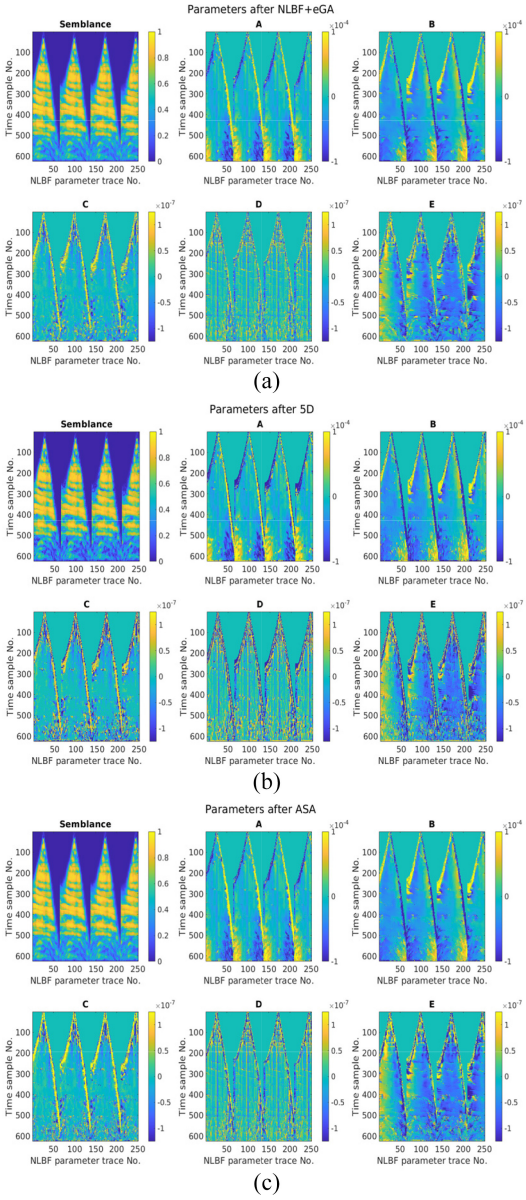

Fig. 4. Estimated semblance values and parameters *A*–*E* for selected NLBF parameter traces obtained by (a) NLBF+eGA method, (b) 5-D brute-force search method, and (c) ASA method on the synthetic example.

The source wavelet is a Ricker wavelet with a dominant frequency of 20 Hz. The time sampling rate is 4 ms, and the record length is 2.5 s. A standard seismic processing procedure known as hyperbolic normal move-out (NMO) correction is further applied to the simulated data to flatten the seismic events. Several raw receiver lines after such correction are shown in Fig. 3(a). Due to the complexities in the near surface, we can easily observe that strong scattering noise contaminates the data, as highlighted by the red oval. The spatial aperture of the NLBF parameter trace for this example is 400 m by 400 m. The spacing between NLBF parameter traces is 140 m in both x and y directions. We select the search ranges of parameters *A*–*E* as follows to focus on reflection events: $A \in [-10^{-4}$ s/m, 10^{-4} s/m], $B \in [-10^{-4}$ s/m, 10^{-4} s/m], $C \in [-1.25 \times 10^{-7}$ s/m^2, 1.25×10^{-7} s/m^2], $D \in [-1.25 \times 10^{-7}$ s/m^2, 1.25×10^{-7} s/m^2], and $E \in [-1.25 \times 10^{-7}$ s/m^2, 1.25×10^{-7} s/m^2]. For this example, the maximum number of evolution generations for the eGA is set at 30. For synthetic data at hand, the NLBF+eGA method

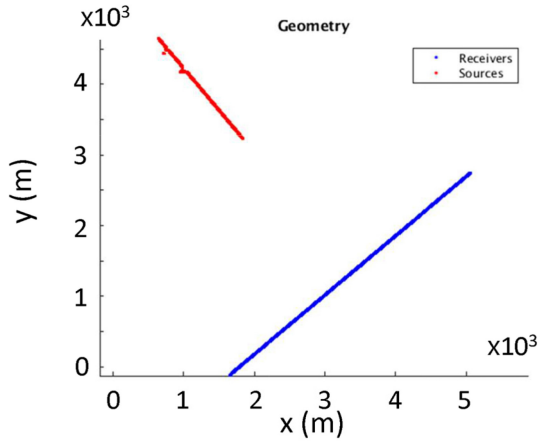

Fig. 5. Source and receiver distributions for a single-sensor cross-spread gather from 3-D land seismic data.

TABLE I
RUNTIME INFORMATION FOR ALL METHODS RUNNING ON THE SYNTHETIC DATASET. THE UNIT IS SECOND

Run No.\ Method	NLBF+eGA	NLBF+eGA (no spatial consistency)	5D	ASA
1	555.07	670.72	814214.49	4469.49
2	554.19	669.93	813446.85	4452.95
3	555.06	669.70	813156.95	4456.72
4	555.30	656.75	812413.38	4611.25
5	556.19	669.67	812503.01	4450.53
6	524.93	670.93	812945.58	4548.07
7	524.49	671.34	815447.58	4532.29
8	554.45	670.20	812522.58	4482.49
9	554.45	671.44	816630.63	4475.20
10	555.24	633.77	814531.13	4523.41

uses the receiver x location as the x-coordinate and the source x location as the y-coordinate in (1). Its corresponding enhanced receiver lines are shown in Fig. 3(b). The data quality improvement is clearly visible, as highlighted by the red oval. The semblance values and parameters *A*–*E* of some NLBF parameter traces are shown in Fig. 4(a). To better appreciate the performance of the NLBF+eGA method, we use the 5-D brute-force search method and the ASA method for performance comparisons. For the 5-D brute-force search method, the search ranges of the parameters *A*–*E* are discretized by small steps, which are set as $\Delta A = \Delta B = 10^{-5}$ s/m and $\Delta C = \Delta D = \Delta E = 2.5 \times 10^{-8}$ s/m^2. For this example, this means that the 5-D brute-force search method has to evaluate (2) for 400 000 times to pick out the best solution as the global minimum for each NLBF operator. The enhanced data and estimated semblance values, along with the parameters *A*–*E* obtained by the 5-D brute-force search method and the ASA method, are shown in Figs. 3(c) and (d) and 4(b) and (c). We can easily observe that both the NLBF+eGA results and the ASA results are very close to those by the 5-D brute-force search method. We run each method ten times to obtain the average runtime for efficiency comparisons. The detailed runtime information can be found in Table I. The 5-D brute-force search method took ~813 781 s of computation time, and the ASA method took ~4500 s. In contrast, the NLBF+eGA method consumed only ~548 s. The NLBF+eGA method delivers a speed-up factor of 1485 over the 5-D brute-force search method and a speed-up factor of 8.21 over the ASA method with similar quality results obtained in this example.

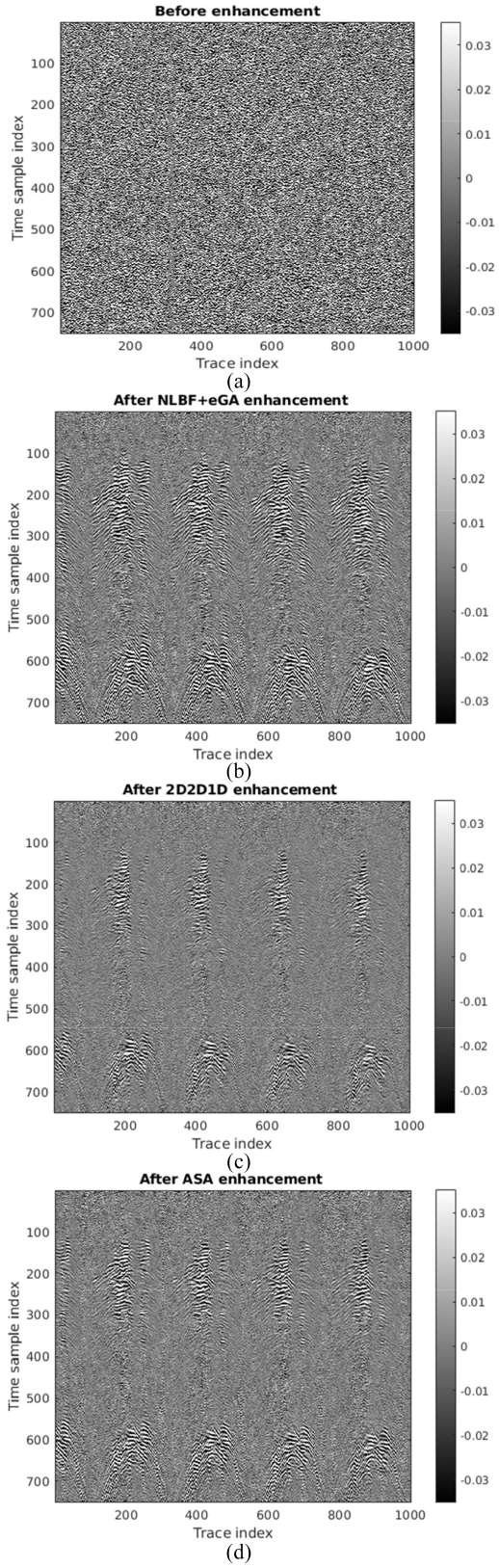

Fig. 6. (a) Several receiver lines extracted from the cross-spread gather of a challenging 3-D single-sensor land seismic dataset. The same receiver lines after enhancement by (b) NLBF+eGA method, (c) conventional NLBF with the 2+2+1 method, and (d) conventional NLBF with the ASA method.

Next, we apply the NLBF+eGA method to a very challenging 3-D single-sensor land seismic dataset acquired in a desert environment. We aim to enhance early arrivals so that on this dataset, reliable

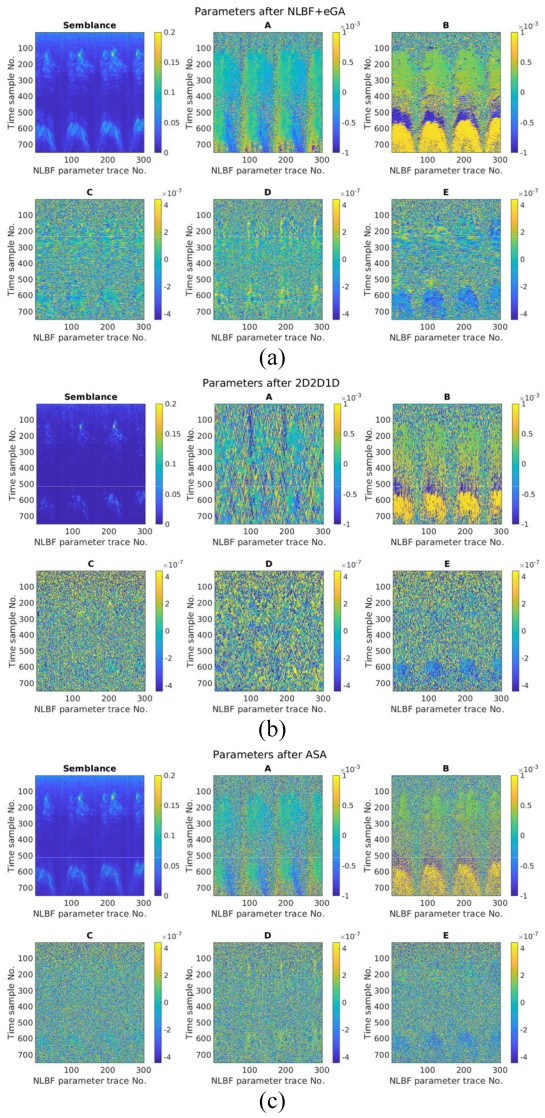

Fig. 7. Estimated semblance values and parameters A–E for selected NLBF parameter traces obtained by (a) NLBF+eGA method, (b) 2+2+1 method, and (c) ASA method on the challenging field dataset.

first-break picking can be performed. Fig. 5 shows the source and receiver distributions of the real data, forming a cross-spread gather introduced in Section II. There are 94 sources and 224 receivers, and both the source and the receiver spacing are 20 m. This dataset is heavily contaminated by near-surface scattering noise. Fig. 6(a) shows some raw traces from nearby receiver lines. No coherent energy can be recognized, illustrating the challenging nature of this dataset. For this example, the spatial aperture of the NLBF parameter trace is 300 m by 300 m, and the spacing between NLBF parameter traces is 50 m in both x and y directions. Since refraction events are of interest in this example, broader search ranges were chosen for parameters A∼E to focus on early arrivals or refraction events: $A \in [-10^{-3}$ s/m, 10^{-3} s/m], $B \in [-10^{-3}$ s/m, 10^{-3} s/m], $C \in [-4.44 \times 10^{-7}$ s/m^2, 4.44×10^{-7} s/m^2], $D \in [-4.44 \times 10^{-7}$ s/m^2, 4.44×10^{-7} s/m^2], and $E \in [-4.44 \times 10^{-7}$ s/m^2, 4.44×10^{-7} s/m^2]. As this is a very challenging dataset, the maximum number of evolution generations for NLBF+eGA is set at 60. The NLBF+eGA method is applied to this data using the receiver station number as the x coordinate and the shot station number as the y coordinate in (1). Gathers after enhancement are shown in Fig. 6(b). The data quality

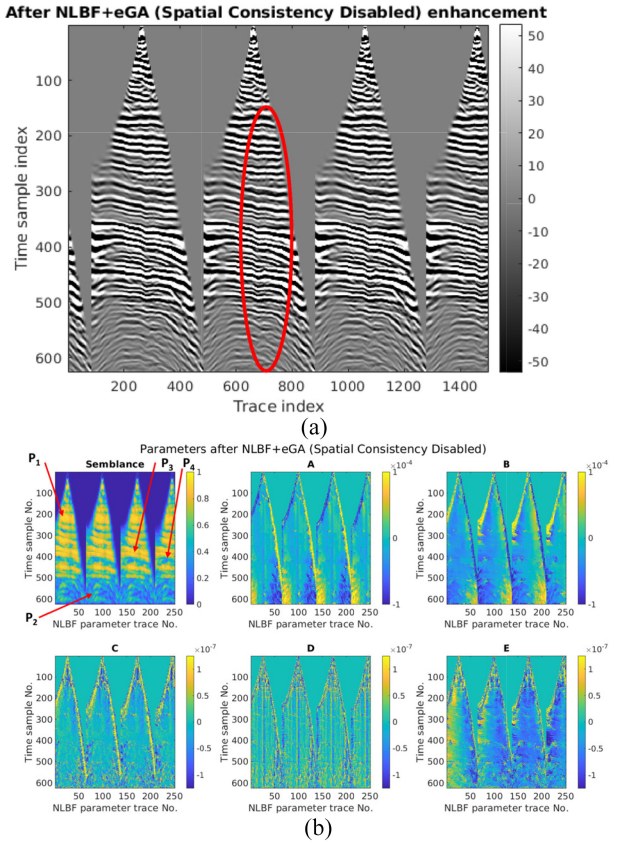

Fig. 8. (a) Same synthetic gathers as shown in Fig. 3 but enhanced using the NLBF+eGA method with the spatial consistency disabled. (b) Estimated semblance values and parameters A∼E for selected NLBF parameter traces obtained by the NLBF+eGA method with the spatial consistency disabled for the synthetic example. Four arrows P_1–P_4 point at four points for comparing semblance evolution between the NLBF+eGA methods with and without the spatial consistency enabled.

improvement is evident with early arrivals and later events distinguished by an eye. The semblance values and parameters A–E of selected NLBF parameter traces are displayed in Fig. 7(a). The 5-D brute-force method becomes computationally unaffordable for this dataset. As such, we use the 2+2+1 method and the ASA method to set the performance control results for better appreciating the performance of the NLBF+eGA method. The discretization steps for the 2+2+1 method in the search ranges of parameters A–E are: $\Delta A = \Delta B = 1.33 \times 10^{-5}$ s/m and $\Delta C = \Delta D = \Delta E = 4.44 \times 10^{-8}$ s/m^2. The enhanced data and estimated parameters by the 2+2+1 method and the ASA method are shown in Figs. 6(c) and (d) and 7(b) and (c). We can observe that results from both the 2+2+1 method and the ASA method are much worse than those from the NLBF+eGA method. Estimated parameters also exhibit jitter for both the 2+2+1 method [Fig. 7(b)] and the ASA method [Fig. 7(c)]. In contrast, they behave better for the NLBF+eGA method [Fig. 7(a)]. Comparing Fig. 6(b)–(d), we note that this improvement translates into better coherency and continuity of events after enhancement by the NLBF+eGA method. The detailed runtime information of each method can be found in Table II. The 2+2+1 method took ∼2496 s of computation time, the ASA method took ∼10757 s, whereas the NLBF+eGA method took ∼2609 s. The NLBF+eGA method clearly outperforms the control methods to deliver much higher quality results efficiently.

TABLE II
RUNTIME INFORMATION FOR ALL METHODS RUNNING ON THE FIELD DATASET. THE UNIT IS SECOND

Run No.\ Method	NLBF+eGA	NLBF+eGA (no spatial consistency)	2+2+1	ASA
1	2597.97	2913.01	2553.16	10902.16
2	2596.67	2790.76	2444.70	10739.15
3	2597.45	2789.40	2439.09	10716.57
4	2596.27	2792.91	2444.51	10687.55
5	2718.92	2909.21	2553.45	10727.36
6	2600.03	2910.62	2444.17	10670.40
7	2596.16	2786.82	2517.66	10811.45
8	2594.32	2913.41	2556.25	10753.25
9	2599.20	2791.13	2558.97	10839.41
10	2593.84	2794.47	2445.93	10726.01

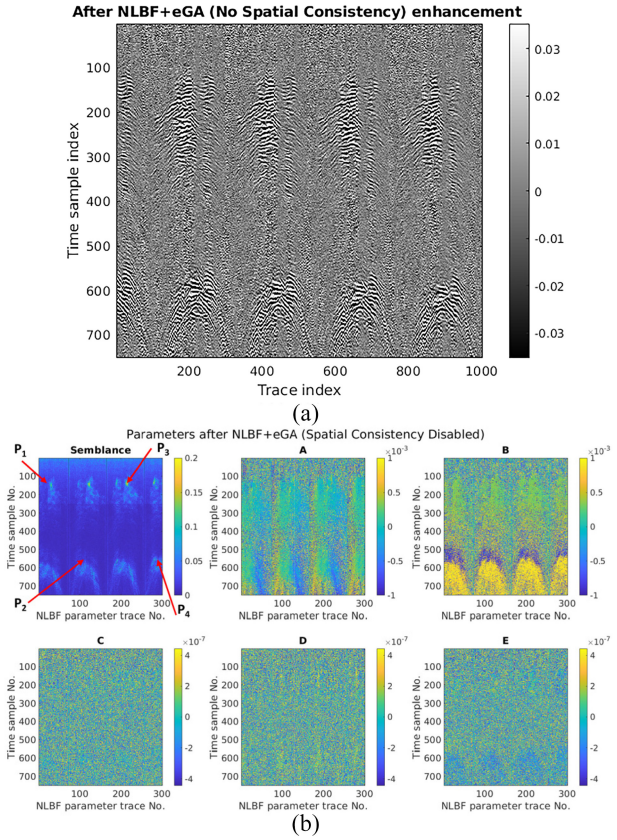

Fig. 9. Same as Fig. 8 but for the challenging field land seismic dataset.

V. DISCUSSION

In Section II, we have introduced our NLBF+eGA method in detail. It contains a novel feature of "spatial consistency" in its algorithm. This section demonstrates this feature's value on both the result quality and the runtime efficiency.

We disable the functionality of "spatial consistency" in the NLBF+eGA method and rerun the two examples in this article using the same parameter settings shown in Section IV, and the corresponding results are shown in Figs. 8 and 9. The detailed runtime information of the NLBF+eGA method without the "spatial consistency" functionality on these two examples can be found in Tables I and II. For the synthetic example, we can observe that Fig. 8 is very close to Figs. 3(b) and 4(a) in terms of the result quality. However, in terms of the computation time, the NLBF+eGA method without

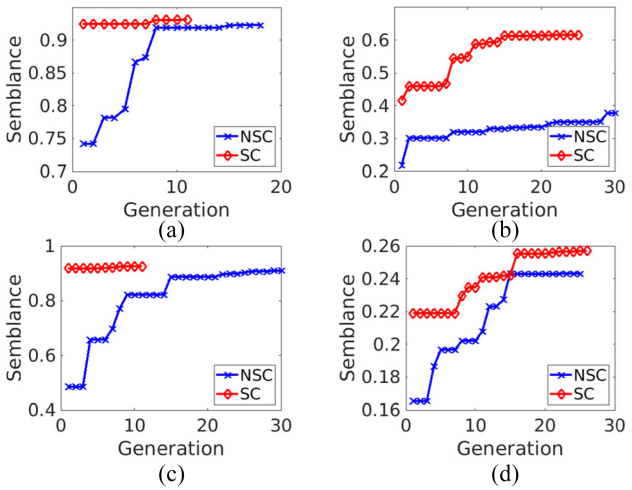

Fig. 10. Semblance improvement relative to evolution generation using the NLBF+eGA methods with (SC) and without (NSC) the spatial consistency enabled for the local traveltime operators at different points marked on Fig. 8(b). (a) P_1. (b) P_2. (c) P_3. (d) P_4.

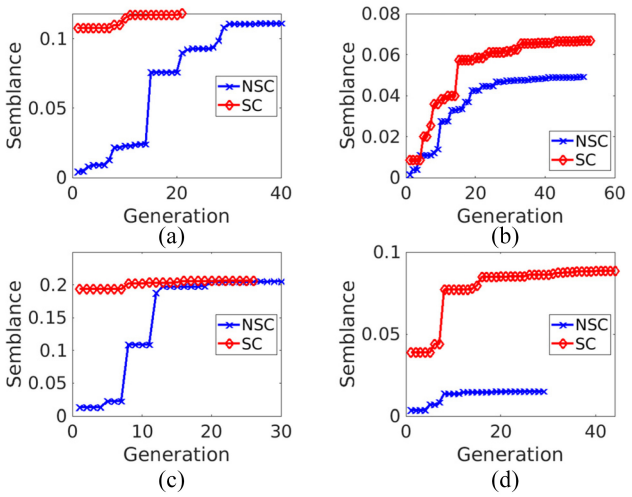

Fig. 11. Same as Fig. 10 but for four local traveltime operators at different points marked on Fig. 9(b). (a) P_1. (b) P_2. (c) P_3. (d) P_4.

the "spatial consistency" functionality took ∼665 s. This comparison shows that with the very similar quality results obtained, the feature of "spatial consistency" yields a speed-up factor of 1.2× on this example. For the field data example, the gathers enhanced without the "spatial consistency" functionality (Fig. 9) appear worse than those shown in Figs. 6(b) and 7(a): fewer coherent events are recovered, and the estimated semblance values are also weaker. In terms of computation time, in this example, the version without the "spatial consistency" functionality took ∼2839 s. In other words, for this field data example, disabling the "spatial consistency" feature in the NLBF+eGA method yields worse results with ∼9% more computation time spent.

We further show comparisons on semblance evolution of local traveltime operators between the NLBF+eGA methods with and without the "spatial consistency" functionality during the optimization process. Figs. 10 and 11 show the semblance improvement relative to evolution generation for four local traveltime operators, pointed out by the red arrows on Figs. 8(b) and 9(b), for the synthetic example and the 3-D field data example. These comparisons show that the "spatial consistency" functionality allows the NLBF+eGA method to start with a better trial solution and to converge generally faster than without it.

VI. Conclusion

The NLBF+eGA method is a novel implementation of NLBF. It applies the eGA to robustly and rapidly find local wavefront attributes in the 5-D parameter space. In addition, it exploits the feature of "spatial consistency" in far-field seismic data to further improve its efficiency. This method's efficacy has been demonstrated using both a synthetic dataset and a challenging single-sensor land seismic dataset from the desert environment. The NLBF+eGA method enables significant improvement in SNR for 3-D seismic data with much less computational effort. It will benefit the seismic processing and interpretation in challenging areas such as the desert environment.

Acknowledgment

The authors are grateful to Maxim Dmitriev (Saudi Aramco) for his help with synthetic forward modeling and Maxim Protasov (IPGG SB RAS) for helping with the algorithm of adaptive simulated annealing.

References

[1] C. Regone, M. Fry, and J. Etgen, "Dense sources vs. dense receivers in the presence of coherent noise: A land modeling study," in *Proc. SEG Expanded Abstracts*, 2015, pp. 12–16.

[2] A. Bakulin *et al.*, "Nonlinear beamforming for enhancing prestack seismic data with a challenging near surface or overburden," *First Break*, vol. 36, no. 12, pp. 121–126, 2018.

[3] A. Bakulin *et al.*, "Nonlinear beamforming for enhancement of 3D prestack land seismic data," *Geophysics*, vol. 85, pp. V283–V296, May 2020.

[4] Y. Zhang, S. Bergler, and P. Hubral, "Common-reflection-surface (CRS) stack for common offset," *Geophys. Prospecting*, vol. 49, no. 6, pp. 709–718, 2001.

[5] Y. P. V. Acuna, Y. Sun, and R. van Borselen, "An enhanced genetic algorithm and its application on nonlinear geophysical problems," in *Proc. 81st EAGE Conf. Exhibit.*, 2019, pp. 1–5.

[6] Y. P. V. Acuna and Y. Sun, "An efficiency-improved genetic algorithm and its application on multimodal functions and a 2D common reflection surface stacking problem," *Geophys. Prospecting*, vol. 68, pp. 1189–1210, May 2020.

[7] A. Berkovitch, K. Deev, and E. Landa, "How nonhyperbolic MultiFocusing improves depth imaging," *First Break*, vol. 27, pp. 95–103, Sep. 2011.

[8] D. E. Goldberg, *Genetic Algorithms in Search, Optimization and Machine Learning*. Boston, MA, USA: Addison-Wesley, 1989.

[9] L. J. Eshelman and J. D. Schaffer, "Real-coded genetic algorithms and interval-schemata," *Found. Genet. Algorithms*, vol. 2, pp. 187–202, Jan. 1993.

[10] P. W. Poon and J. N. Carter, "Genetic algorithm crossover operators for ordering applications," *Comput. Oper. Res.*, vol. 22, pp. 135–147, Jan. 1995.

[11] Y.-C. Chuang, C.-T. Chen, and H. Hwang, "A simple and efficient real-coded genetic algorithm for constrained optimization," *Appl. Soft Comput.*, vol. 38, pp. 87–105, Jan. 2016.

[12] D. M. Pierre and N. Zakaria, "Stochastic partially optimized cyclic shift crossover for multi-objective genetic algorithms for the vehicle routing problem with time-windows," *Appl. Soft Comput.*, vol. 52, pp. 863–876, Mar. 2017.

[13] Y. Gong and A. Fukunaga, "Distributed island-model genetic algorithms using heterogeneous parameter settings," Presented at the IEEE Congr. Evol. Comput., New Orleans, LA, USA, Jun. 2011, pp. 820–827.

[14] K. Deep and M. Thakur, "A new mutation operator for real coded genetic algorithms," *Appl. Math. Comput.*, vol. 193, pp. 211–230, Oct. 2007.

[15] K. Li, Á. Fialho, S. Kwong, and Q. Zhang, "Adaptive operator selection with bandits for a multiobjective evolutionary algorithm based on decomposition," *IEEE Trans. Evol. Comput.*, vol. 18, no. 1, pp. 114–130, Feb. 2014.

[16] E. Shojaedini, M. Majd, and R. Safabakhsh, "Novel adaptive genetic algorithm sample consensus," *Appl. Soft Comput.*, vol. 77, pp. 635–642, Apr. 2019.
[17] S. W. Mahfoud, "Crowding and preselection revisited," in *Parallel Problem Solving from Nature 2*. Amsterdam, The Netherland: North-Holland Publ. Company, 1992, pp. 27–36.
[18] J. Horn, "Finite Markov Chain analysis of genetic algorithms with niching," in *Proc. 5th Int. Conf. Genet. Algorithms*, 1993, pp. 110–117.
[19] S. Pierini, M. Aleardi, and A. Mazzotti, "A method to attenuate genetic drift in genetic-algorithm optimizations: Applications to analytic objective functions and two seismic optimization problems," *Geophysics*, vol. 84, no. 2, pp. R295–R310, 2019.
[20] M. Jervis, M. K. Sen, and P. L. Stoffa, "Prestack migration velocity estimation using nonlinear methods," *Geophysics*, vol. 60, no. 1, pp. 138–150, 1996.
[21] I. Akça and A. T. Basokur, "Extraction of structure-based geoelectric models by hybrid genetic algorithms," *Geophysics*, vol. 75, no. 1, pp. F15–F22, 2010.
[22] Y. Sun and D. J. Verschuur, "A self-adjustable input genetic algorithm for the near-surface problem in geophysics," *IEEE Trans. Evol. Comput.*, vol. 18, no. 3, pp. 309–325, Jun. 2014.
[23] Y. Sun, E. Verschuur, and J. W. Vrolijk, "Solving the complex near-surface problem using 3D data-driven near-surface layer replacement," *Geophys. Prospecting*, vol. 62, pp. 491–506, May 2014.
[24] Y. Sun, E. Verschuur, and Y. Luo, "Research Note: Near-surface layer replacement for sparse data: Is interpolation needed?" *Geophys. Prospecting*, vol. 65, pp. 1694–1705, Nov. 2017.
[25] M. Aleardi and A. Mazzotti, "1D elastic full-waveform inversion and uncertainty estimation by means of a hybrid genetic algorithm," *Geophys. Prospecting*, vol. 65, no. 1, pp. 64–85, 2016.
[26] C. Stork and T. Kusuma, "Hybrid genetic autostatics: New approach for large-amplitude statics with noisy data," in *Proc. SEG Expanded Abstracts,* 1992, pp. 1127–1131.
[27] Y. Sun, T. Tonellot, B. Kamel, and A. Bakulin, "A 2D automatic converted-wave static-correction algorithm," *Leading Edge*, vol. 35, no. 3, pp. 280–284, 2016.
[28] Y. Sun, Y. Sun, T. Tonellot, B. Kamel, and A. Bakulin, "A two-phase automatic static correction method," *Geophys. Prospecting*, vol. 65, no. 3, pp. 711–723, 2017.
[29] M. Oristaglio, "SEAM update," *Leading Edge*, vol. 34, no. 10, pp. 466–468, 2015.
[30] L. Ingber, "Adaptive simulated annealing (ASA): Lessons learned," *Control Cybern.*, vol. 25, no. 1, pp. 32–54, 1996.